Liquid Structure of Acetic Acid Studied by Raman Spectroscopy and Ab Initio Molecular Orbital Calculations

Takakazu Nakabayashi,[†] Kentaroh Kosugi,[‡] and Nobuyuki Nishi*[,†,‡]

Institute for Molecular Science, and School of Mathematical and Physical Science, The Graduate University for Advanced Studies, Okazaki National Research Institutes, Myodaiji, Okazaki 444-8585, Japan

Received: May 6, 1999; In Final Form: July 12, 1999

The liquid structure of acetic acid was studied experimentally and theoretically. Experimentally, the Raman spectra of acetic acid at various temperatures between 287 and 348 K were measured in the region 15−3700 cm^{-1}. Theoretically, ab initio molecular orbital calculations were performed on the Raman activities of seven cluster species of acetic acid molecules. The Raman spectrum (in $R(\bar{\nu})$ representation) of crystalline acetic acid at 287 K shows six distinct bands in the 15−300 cm^{-1} region. These bands broaden on the melting of the crystal, whereas their peak positions remain almost unchanged on melting. These spectral changes are reproduced in the case where the liquid spectrum mainly arises from a variety of sizes of chain clusters as the fragments of the crystalline networks. The C═O stretching band becomes broadened toward higher wavenumbers and exhibits an asymmetric shape with increasing temperature. The wavenumbers calculated for the C═O stretching vibrations suggest that the strongly hydrogen-bonded C═O groups of the chain clusters show the prominent C═O band and its asymmetric shape is due to the presence of weakly hydrogen-bonded C═O groups of the same cluster species. The spectral analyses in both the low wavenumber and the C═O stretching regions suggest that liquid acetic acid is mainly composed of the chain clusters, not the cyclic dimer. Assignments of the low-frequency Raman bands observed in the vapor and crystalline states are discussed on the basis of the calculated wavenumbers.

1. Introduction

Molecules with carboxylic groups show specific hydrogen-bonding interactions with each other or with other hydrogen-donating or -accepting molecules. To understand their unique ability to form associates through hydrogen bonds, the molecular association of acetic acid has long been studied as a prototype system of carboxylic compounds. Because acetic acid has four hydrogen-donor sites (a hydroxyl hydrogen and three methyl hydrogens) and two acceptor sites (a hydroxyl oxygen and a carboxyl oxygen) in a molecule, various kinds of associations of acetic acid molecules can be expected in various situations. In the vapor phase, acetic acid exists in a mixture of two species, monomers and dimers, at temperatures <150 °C.[1,2] The latter dimer formed by hydrogen-bonding is known to have a planar ring structure of C_{2h} symmetry from electron diffraction studies.[3,4] This dimer is therefore called a cyclic dimer. Some other carboxylic acids are also shown to form such cyclic dimers in the gas phase.[3,5,6]

In the crystalline state, on the other hand, acetic acid exists in infinite chains that involve C−H···O═C and O−H···O═C hydrogen bonds, as depicted in Figure 1.[7−9] Although the C···O distance of 3.429 Å[9] is longer than those of the O−H···O and N−H···O hydrogen bonds, Taylor and Kennard[10] provided evidence for the existence of the C−H···O═C hydrogen bond by analyzing neutron diffraction data. Such a C−H···O hydrogen bond has been known to contribute significantly to the stability of acetic acid and other molecular crystals.[11] Crystalline acetic acid has a melting point at 289.8 K. X-ray diffraction data collected at 278 and 83 K have shown that the hydrogen bond lengths do not vary with the temperature, whereas minor changes occur in the packing of the hydrogen-bonded chains.[9] Formic acid is also shown to form similar infinite chains in the crystalline state,[10] but other carboxylic acids, such as propionic and monofluoroacetic acids, exist in the cyclic dimers as in the gas phase.[13−15]

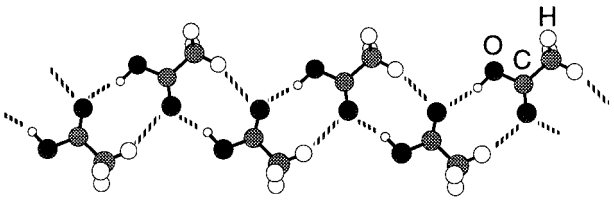

Figure 1. Orientation of acetic acid molecules in the crystalline network structure derived from refs 7−9.

The liquid structure of acetic acid is also considered to be determined mainly by hydrogen-bonding interactions. Information on the liquid structure is, however, more limited than that on the gas and the crystalline network structures, which can be derived from electron and X-ray diffraction measurements, respectively. Bertagnolli and Hertz have performed neutron and X-ray diffraction measurements on liquid acetic acid.[16,17] They found the remarkable constancy of the hydrogen bond length as the substance passes from the crystalline to the liquid state.[16] Comparison of the simulated results based on the crystal-like cyclic dimer structure and the chain structure existing in the crystalline state suggested that the cyclic dimer structure yields a better description of the structure of liquid acetic acid.[17] However, other structures, such as chain "fragments" of the crystalline networks, were not treated in the report.[17]

* To whom correspondence should be addressed. Fax: +81-564-54-2254. E-mail: nishi@ims.ac.jp.
† Institute for Molecular Science.
‡ The Graduate University for Advanced Studies.

10.1021/jp991501d CCC: $18.00
Published on Web 10/14/1999

Low-frequency vibrational spectroscopy is very useful for studies of local structures of solution systems because it directly probes intermolecular vibrational bands. Far-infrared (far-IR) and low-frequency Raman spectra of liquid acetic acid have been observed by several groups including ourselves.[18−23] Waldstein and Blatz observed the low-frequency Raman spectra of liquid acetic acid and suggested that the cyclic dimers are predominant structures in the liquid state.[19] Their analysis was based on the normal coordinate calculations with empirical force constants.[24] Nielsen and Lund[20] assigned the three distinctive peaks of the Raman spectrum of the liquid to the three fundamental modes of the cyclic dimer by means of depolarization ratios, isotope effects, and the calculations with empirical force fields.[23−26] Their assignments, however, were based on the assumption that all the bands observed in the liquid spectra arise from the cyclic dimer. To the best of our knowledge, no one has analyzed the low-frequency Raman spectra of acetic acid on the basis of the calculations for the chain fragments of crystalline networks.

In the present paper, the structure of liquid acetic acid is reinvestigated experimentally and theoretically. To make complete analyses of not only intermolecular but also intramolecular vibrations, we examined the Raman spectra of acetic acid in a wide wavenumber region of 15−3700 cm^{-1}. We also performed ab initio molecular orbital (MO) calculations on the Raman spectra of some different cluster species of acetic acid molecules. The Raman band intensities of the cluster species were compared with the observed spectra to clarify the structure of liquid acetic acid. A preliminary account of this study has been published elsewhere.[21] Details of the theoretical results including more advanced treatments and analyses of the spectra in a high wavenumber region are contained in this paper.

2. Materials and Methods

Spectroscopy grade acetic acid was purchased from Wako Pure Chemical Company and used without further purification. Sample solutions were sealed in $\Phi = 6$ mm Pyrex glass tubes after deaerating of carbon dioxide by repeating freezing and evacuation. Crystalline samples were grown in tapered glass tubes in a commercial refrigerator. Silicon rubber heaters wound on the sealed glass tube were used for temperature control. The temperature of the sample was monitored by a thermocouple placed ≈1 mm down from the laser point. The Raman spectra were obtained with the 514.527 nm line from an Ar^+ ion laser (NEC). The Raman-scattered light at 90° was analyzed by an NR-1800 Raman spectrometer (JASCO) equipped with a triple monochromator and a thermoelectrically cooled photomultiplier tube (Hamamatsu Photonics R943−02). The incident laser was linearly polarized, and neither a polarizer nor a polarization scrambler was used to keep the throughput of the spectrometer as high as possible. Polarization dependency of the sensitivity of the spectrometer was separately examined with the Raman bands of carbon tetrachloride and cyclohexane and was found to be <10%. The average power of the exciting light was ≈150 mW at the sample.

Ab initio MO calculations were performed with the Gaussian 94 program package[27] on a DEC workstation (AlphaStation 500). All the calculations were carried out at the Hartree−Fock (HF) level. The 6-31G** basis set was employed. The 6-31++G** basis set, which contains one set of diffuse functions on all the atoms, was also employed, with the exception of the pentamer.

At the HF level, the acetic acid molecules were optimized to have a C_s plane containing the heavy atoms and one of the methyl hydrogen at the side of the C═O group. The other two methyl hydrogens are located symmetrically above and under the carboxylic plane. A planar structure of C_s symmetry was assumed for each cluster species. Force calculations confirmed convergence to the minima on the potential energy surface because the wavenumbers of all the modes were real for the optimized structures of the monomers and the cluster species.

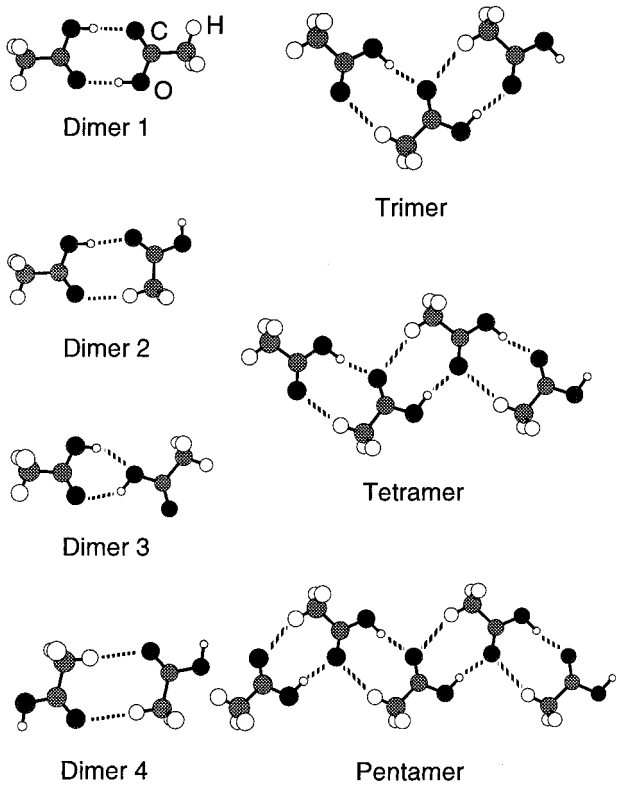

Figure 2. Optimized geometries of acetic acid cluster species treated in this study.

3. Results and Discussion

3.A. Calculated Structures and Hydrogen-Bonded Energies of Cluster Species. The structures of the cluster species treated in this study are shown in Figure 2. Two conformers must be considered for acetic acid: the hydroxyl hydrogen and the carbonyl oxygen on the same side (*syn*) and on the opposite side (*anti*). The ab initio MO calculations predict that *syn*-conformer of acetic acid is more stable than *anti*-conformer by 7.0 kcal/mol at the HF/6-31++G** level. Such an energy difference may arise from a weak internal hydrogen bond between the hydroxyl hydrogen and the carbonyl oxygen in the *syn* form. Because the *syn*-conformers are observed in both the gas and crystalline phases as dominant structures, the *anti*-conformers are considered to be not so important in the liquid state. Hence only the cluster species of the *syn*-conformers are treated in this study.

Four dimer species are taken into account for the calculation, all of which contain two intermolecular hydrogen bonds. Dimer 1 contains two O−H···O═C hydrogen bonds and has C_{2h} symmetry. This dimer is dominant in the gas phase at temperatures <150 °C[3,4] and is called the cyclic dimer as already mentioned. In dimer 2, one of the O−H···O═C hydrogen bonds in dimer 1 is replaced by a C−H···O═C hydrogen bond. This dimer can be regarded as the dimer unit of the chain structure in the crystal shown in Figure 1. Dimer 3 contains one

TABLE 1: Incremental Hydrogen-Bonding Energies of Acetic Acid Aggregates

method	aggregate	hydrogen-bonding energy /kcal mol^{-1} without corr.	after ZPVE
HF/6-31G**	dimer 1	−15.50	−13.96
	dimer 2	−8.79	−7.69
	dimer 3	−7.36	−6.37
	dimer 4	−3.36	−2.73
	trimer	−9.02	−8.04
	tetramer	−9.20	−8.22
	pentamer	−9.24	−8.26
HF/6-31++G**	dimer 1	−13.86	−12.31
	dimer 2	−7.82	−6.75
	dimer 3	−6.24	−5.27
	dimer 4	−2.71	−2.14
	trimer	−8.10	−7.09
	tetramer	−8.27	−7.28

O−H···O═C hydrogen bond and one additional intermolecular hydrogen bond between the acidic hydrogen and the oxygen atom of the OH group. This structure is suggested to be formed in aqueous solutions on the basis of several experimental facts.[28−31] Dimer 4 is a cyclic complex with two C−H···O═C hydrogen bonds and has C_{2h} symmetry. Various kinds of cluster species of acetic acid molecules can be formed in combination with these four dimer species. Trimer, tetramer, and pentamer, all of which structures are calculated as the chain fragments of the hydrogen-bonded networks of the crystal (Figure 1).

Table 1 shows the incremental hydrogen-bonding energies of the optimized geometries of the cluster species. Corrected energies for zero-point vibrational energies (ZPVE) are also shown in Table 1. Dimer 1 is the most stable among the four dimer species, as expected. As for the chain fragments of the crystalline networks, the hydrogen-bonding energy increases with increasing aggregate size. Turi and Dannenberg have shown that this stabilization is due to the increase in the cooperative interactions between acetic acid molecules with increasing aggregation.[31,33] They also estimated the hydrogen-bonding energy expected for the infinite chain by an asymptotical approach. At the HF/6-31G** level, this value was estimated to be −9.85 kcal/mol without corrections, and −8.4 kcal/mol after correction for ZPVE.[31,33] This difference indicates that, even for the pentamer, the calculated hydrogen-bonding energy is smaller than that for the infinite chain. For all the aggregates, HF/6-31++G** predicts a lower hydrogen-bonding energy than HF/6-31G**.

The optimized geometrical parameters of the monomer and the dimer species at the HF/6-31++G** level are collected in Table 2. Dimer 1 has the shortest C−O bond length, the longest C═O and O−H bond lengths, and the shortest O···O distance for the O−H···O═C hydrogen bond. This result indicates that the O−H···O═C hydrogen-bonding interaction of dimer 1 is the strongest, as far as the dimer species are concerned. Dimer 2 has a shorter C···O distance for the C−H···O═C hydrogen bond than dimer 4. This result means that the C−H···O═C interaction of dimer 2 is stronger than that of dimer 4. The C−H bond lengths of all the dimer species remain almost constant even in the presence of hydrogen-bonding interactions.

Table 3 shows the optimized structures of the chain fragments characteristic of hydrogen-bonding interactions. To simplify the analyses of the optimized parameters of the chain clusters, the averaged values for the constituent acetic acid molecules are shown in this table. The trends of the geometrical change with increasing cluster size have been also found by Turi and Dannenberg.[33] The most interesting to note is that the O···O

TABLE 2: Calculated Geometrical Parameters[a] of Acetic Acid Monomer and Dimer Species at the HF/6-31++G Level**

parameter	monomer	dimer 1	dimer 2[b]		dimer 3[c]		dimer 4
r(C═O)	1.189	1.203	1.195	1.197	1.196	1.187	1.192
r(C−O)	1.331	1.308	1.318	1.324	1.323	1.333	1.331
r(O−H)	0.949	0.962	0.958	0.949	0.952	0.956	0.948
r(C−C)	1.501	1.500	1.503	1.498	1.500	1.502	1.499
r(C−H)[d]	1.079	1.079	1.080	1.079	1.079	1.079	1.079
r(C−H)[e]	1.084	1.084	1.084	1.084	1.084	1.084	1.084
r(O···O)[f]		2.793	2.860			2.818	
r(O···O)[g]					2.999		
r(C···O)[h]				3.500			3.634
α(O−C═O)	122.16	123.28	123.23	121.20	122.70	122.39	121.69
α(C−C═O)	125.68	123.66	124.44	125.86	124.80	125.44	125.89
α(C−O−H)	108.93	111.28	111.08	109.23	110.30	111.34	108.86

[a] In units of angstrom (bond length) and degree (bond angle). [b] First entry is the acetic acid molecule whose OH is the H-bond donor. [c] First entry is the acetic acid molecule whose C═O is the H-bond acceptor. [d] H is in the plane of the heavy atoms. [e] H is out of the plane of the heavy atoms. [f] Intermolecular O···O distance for the O−H···O═C hydrogen bond. [g] Intermolecular O···O distance for the O−H···O−C hydrogen bond. [h] Intermolecular C···O distance for the C−H···O═C hydrogen bond

distance for the O−H···O═C hydrogen bond decreases with increasing extent of aggregation, whereas the C···O distance for the C−H···O═C hydrogen bond increases. In other words, the O−H···O═C interaction becomes stronger and the C−H···O═C interaction becomes weaker as the chain length is extended. The increase in the cooperative interactions shown in Table 1 is therefore the sum of two divergent components.[33] For all the hydrogen bonds, HF/6-31++G** predicts a longer intermolecular distance than HF/6-31G**. This result is in accord with the fact that the hydrogen-bonding energy at the HF/6-31++G** level is lower than that at the HF/6-31G** level for all the aggregates shown in Table 1.

3.B. Observed Low-Frequency Raman Spectra. Figure 3A shows the low-frequency spectra of scattered light intensity ($I(\bar{\nu})$) for acetic acid taken at different temperatures around the melting point (289.8 K). The spectra taken at both 287 and 288 K are due to crystalline acetic acid, the spectrum at 289 K is due to a mixture of solid and liquid acetic acid, and the spectrum at 296 K is due to liquid acetic acid. Although the range of the temperature difference is very small (<9 K), the features observed in the $I(\bar{\nu})$ spectra show marked changes with increasing temperature. In the crystalline spectra taken at both 287 and 288 K, there are six distinct bands: three strong Raman peaks at 50, 124, and 181 cm^{-1}, two weak peaks at 78 and 90 cm^{-1}, and a shoulder at 41 cm^{-1}. The features of these two spectra are almost the same, although the intensity at the low-frequency tail (<80 cm^{-1}) of the Rayleigh scattering signal is slightly larger in the spectrum at 288 K. The intensity of the Rayleigh wing component of the mixture of solid and liquid acetic acid at 289 K increases in comparison with the crystalline spectra, whereas the peak intensities of the three strong Raman bands decrease eminently. In the liquid spectrum at 296 K, the Rayleigh wing component dramatically increases to make it difficult to distinguish the Raman bands from the Rayleigh background. Such a large enhancement of the intensity at the tail of Rayleigh scattering on melting has been observed in other molecular crystals.[34] This phenomenon has been considered to arise from the increase in the density fluctuation with increasing temperature.[35] The problems caused by the very strong Rayleigh line can be partly overcome using the so-called $R(\bar{\nu})$ representation as follows.[20,21,34,36−39]

TABLE 3: Averaged Geometrical Parameters[a] Characteristic of Hydrogen-Bonding Interactions in Chain Clusters of Acetic Acid

method	aggregate	r(C═O)	r(C−O)	r(O−H)	r(O···O)[b]	r(C···O)[c]
HF/6-31G**	dimer 2	1.195	1.320	0.953	2.855	3.461
	trimer	1.197	1.316	0.955	2.825	3.517
	tetramer	1.199	1.314	0.957	2.812	3.535
	pentamer	1.199	1.312	0.958	2.805	3.547
HF/6-31++G**	dimer 2	1.196	1.321	0.954	2.860	3.500
	trimer	1.199	1.317	0.956	2.829	3.557
	tetramer	1.200	1.315	0.957	2.816	3.577

[a] In units of angstrom (bond length) and degree (bond angle). [b] Intermolecular O···O distance for the O—H···O═C hydrogen bond. [c] Intermolecular C···O distance for the C—H···O═C hydrogen bond.

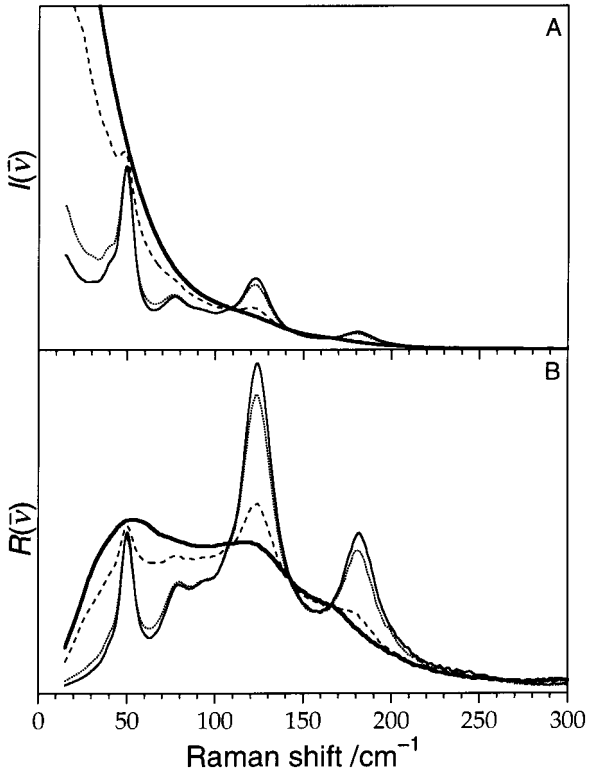

Figure 3. Raman spectra of acetic acid in the 15−300 cm^{-1} region in $I(\bar{\nu})$ (A) and $R(\bar{\nu})$ (B) representations at different temperatures: solid trace, 287 K; dotted trace, 288 K; thick-dotted trace, 289 K; thick-solid trace, 296 K.

The measured scattered light intensity $I(\bar{\nu})$ under the thermal equilibrium is given by the following formula:[36]

$$I(\bar{\nu}) \propto (\bar{\nu}_o - \bar{\nu})^4 \bar{\nu}^{-1} B(\bar{\nu})^{-1} S(\bar{\nu}) \quad (1)$$

$$B(\bar{\nu}) = 1 - \exp\left(-\frac{hc\bar{\nu}}{kT}\right) \quad (2)$$

where $\bar{\nu}_o$ is the excitation wavenumber; $\bar{\nu}$ is the wavenumber of the scattered light; k, h, and c denote the Boltzmann and the Planck constants, and the velocity of light, respectively; T is the vibrational temperature of the sample; $S(\bar{\nu})$ is the sum of the square of the polarizability derivatives with respect to the normal coordinate; and B is the Boltzmann factor. As shown in eqs 1 and 2, the measured intensity $I(\bar{\nu})$ is dependent on the temperature and the scattered wavenumber. This dependence highly affects the low-frequency Raman spectra of noncrystalline states, such as the enhancement of the Rayleigh wing component. To remove these undesirable effects, the reduced function,

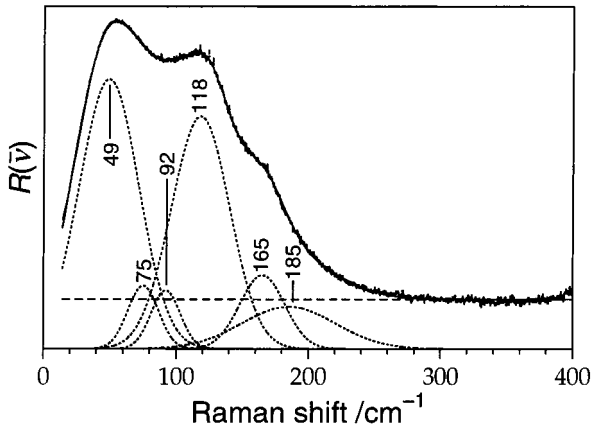

Figure 4. Curve fitting analysis using Gaussian components for $R(\bar{\nu})$ spectrum of liquid acetic acid in the 15−400 cm^{-1} region: dotted trace, observed; solid curve, fitted spectrum with six Gaussian components (thick-dotted curves) and a flat background (broken line). The numbers in the figure indicate peak positions of the Gaussian components.

$R(\bar{\nu})$ is defined as follows:

$$R(\bar{\nu}) = I(\bar{\nu})(\bar{\nu}_o - \bar{\nu})^{-4} \bar{\nu} B(\bar{\nu}) \quad (3)$$

It is noted in eqs 1 and 3 that the $R(\bar{\nu})$ representation provides the corrected Raman intensity that is directly proportional to the intrinsic Raman scattering activity $S(\bar{\nu})$.[36] This representation has the practical advantage of essentially removing the intensity of the exciting laser line and extracting from the measured Raman spectrum a quantity that is related to the vibrational density of states.[20,21,34,36−39] Temperature dependence of the $R(\bar{\nu})$ spectra of acetic acid is shown in Figure 3B. Liquid acetic acid at 296 K exhibits two peaks and one shoulder in the $R(\bar{\nu})$ spectrum, although they are hardly identified in the $I(\bar{\nu})$ spectrum in Figure 3A.

The two $R(\bar{\nu})$ spectra of crystalline acetic acid in Figure 3B are essentially the same. On the other hand, the peak intensities observed in the spectrum of the mixture of solid and liquid acetic acid are much smaller than those in the crystalline spectra. In the liquid spectrum, all the bands broaden and the intensity in the low wavenumber region around 50 cm^{-1} increases, although the positional changes of the two prominent bands at 50 and 124 cm^{-1} are very small on the melting of the crystal. X-ray and neutron scattering measurements have suggested that the hydrogen-bonded atomic distances are preserved during melting.[16] The constancy of the peak position in Figure 3B appears to be in agreement with the X-ray and neutron scattering observations. The band at 181 cm^{-1} seems to shift slightly to a lower wavenumber on the melting. Figure 4 shows the curve fitting analysis for the $R(\bar{\nu})$ spectrum of liquid acetic acid at 296 K. The fit to the liquid spectrum shown in Figure 4 is based on a model composed of six Gaussian line shapes and a flat

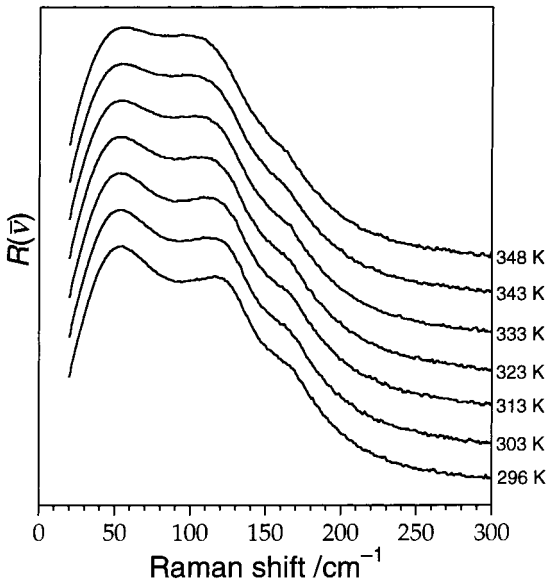

Figure 5. The $R(\bar{\nu})$ spectra of liquid acetic acid in the 15−400 cm^{-1} region at the temperatures of 296, 303, 313, 323, 333, 343, and 348 K. The intensity of each spectrum is normalized by reference to the peak intensity of the band at 50 cm^{-1}.

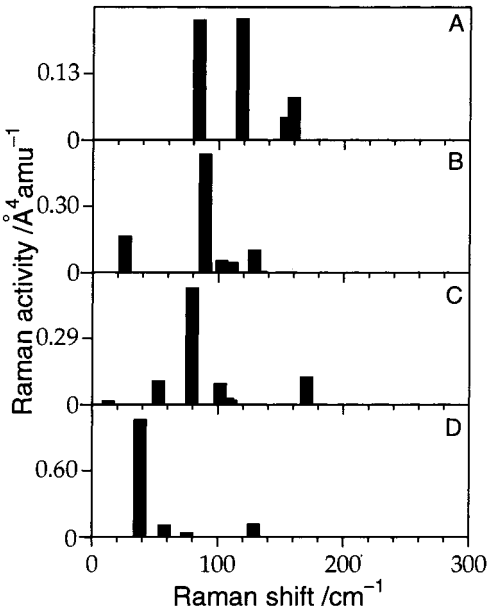

Figure 6. The $R(\bar{\nu})$ spectra in the 0−300 cm^{-1} region calculated for (A) dimer 1, (B) dimer 2, (C) dimer 3, and (D) dimer 4 at the HF/6-31G** level.

background. Inclusion of two Gaussian components at 75 and 92 cm^{-1} is needed to satisfactorily reproduce the liquid spectrum in the 50−200 cm^{-1} region.[21] It should be noted in Figure 4 that the fitting analysis shows the presence of the hidden component with a peak at ≈185 cm^{-1}, the integrated intensity of which is comparable to that of the discernible component at 165 cm^{-1}. This result suggests that the positional change of the 181 cm^{-1} band is also small on the melting. It may therefore be said that the band positions observed in the crystalline spectrum remain almost unchanged on the melting of the crystal.

Figure 5 shows the temperature dependence of the $R(\bar{\nu})$ spectra of liquid acetic acid in the 15−400 cm^{-1} region. The intensity of each spectrum is normalized to the peak intensity of the band at 50 cm^{-1}. The intensities of the bands at 120 and 170 cm^{-1} relative to the band at 50 cm^{-1} increase and show small shifts to lower wavenumbers as the temperature grows. The widths of bands become broader with increasing the temperature, making it difficult to analyze the temperature dependence of the six Gaussian components individually.

3.C. Comparison between Calculated and Observed Low-Frequency Raman Spectra. The $R(\bar{\nu})$ spectra in the 0−300 cm^{-1} region calculated for the dimer species using HF/6-31G** are shown in Figure 6. Table 4 summarizes calculated vibrational wavenumbers and the assignment of these species in the 0−300 cm^{-1} region. The band positions observed in crystalline, liquid, and gaseous acetic acid[40,41] are collected in Table 5. We also calculated the $R(\bar{\nu})$ spectra for the cluster species with the exception of the pentamer at the HF/6-31++G** level, and found that the inclusions of diffuse functions do not seriously affect their peak positions and intensity patterns. In the Gaussian program, the Raman activity ($A(\bar{\nu})$, in units of $Å^4$ amu^{-1}) is defined as proportional to the sum of the square of the polarizability derivatives. Thus we obtained $R(\bar{\nu})$ spectra by plotting $A(\bar{\nu})$ against the calculated wavenumber. Torii and Tasumi have shown that the features observed in the $R(\bar{\nu})$ spectra of hydrogen-bonded amides are well reproduced at the HF level.[37,38] The calculated low wavenumbers are not multiplied by a scale factor because a reliable value of a scale factor for intermolecular vibrations has not been established.

The reported low-frequency Raman spectra of the cyclic dimer in the gas phase at 21 °C showed two broad bands at 106 and 155 cm^{-1}, the former of which was larger in intensity than the latter.[40,41] On the other hand, the ab initio MO calculations for dimer 1 provide four Raman active vibrations in the 0−400 cm^{-1} region. As shown in Figure 6A, the two bands at 84.1 and 118.5 cm^{-1} are comparably strong and the other two bands at 153.7 and 159.5 cm^{-1} are weak. This result may suggest that the broad band at 106 cm^{-1} observed in the vapor state is composed of the two bands, which are assigned to the CH_3 torsion and the out-of-plain ring bent modes, and the 155 cm^{-1} band is also divided in the two bands, which are the hydrogen-bond stretching and the in-plane ring deformation modes. With the help of the normal coordinate calculations with empirical force constants,[23−26] Nielsen and Lund assigned the three peaks at 55, 115, and 165 cm^{-1} in the liquid spectrum to the three fundamental modes of the cyclic dimer, in-plane ring deformation, out-of-plane bent, and hydrogen-bond stretching vibrations, respectively.[20] The ab initio MO calculation for dimer 1, however, predicts that the wavenumber of the in-plane ring deformation mode is the highest among the intermolecular modes.

For all the dimer species in Table 4, the out-of-plane motion of oxygen atoms produces the strongest Raman intensities among the intermolecular modes. Dimer 1 has the highest wavenumber of the strongest Raman active mode among the calculated dimer species, whereas dimer 4 has the lowest one. This result is in accord with the fact that the O−H···O═C hydrogen-bonding interaction of dimer 1 is the strongest and the C−H···O═C interaction of dimer 4 is the weakest among other intermolecular bonds in Table 2. The free CH_3 torsions of dimers 2 and 3 are calculated to be lower in wavenumber than the hydrogen-bonded CH_3 torsions of dimers 2 and 4, but higher than the CH_3 torsions of dimer 1. This result may arise from the situation that the C−H···O═C hydrogen bonds hinder the CH_3 torsional motions and the strong O−H···O═C hydrogen bond of dimer 1 weakens an internal hydrogen bond between the methyl hydrogen in the carboxylic plane and the carbonyl oxygen.

TABLE 4: Calculated Low Wavenumbers (cm^{-1}) of Acetic Acid Dimer Species at the HF/6-31G Level**

dimer 1	dimer 2	dimer 3	dimer 4	assignment[a]
50.2 (0.00)[b]	38.1 (0.00)	13.1 (0.02)	19.4 (0.00)	o.o.p. ring bent
73.2 (0.00)	25.8 (0.17)	52.7 (0.11)	30.8 (0.00)	o.o.p. ring def.
84.1 (0.24)	102.5 (0.05)	101.8 (0.09)		(free) CH_3 tor.
92.1 (0.00)		110.1 (0.02)		(free) CH_3 tor.
	128.5 (0.10)		129.0 (0.12)	(H-bonded) CH_3 tor.
			140.6 (0.00)	(H-bonded) CH_3 tor.
118.5 (0.24)	89.3 (0.54)	79.2 (0.51)	38.2 (1.06)	o.o.p. ring bent
	89.7 (0.05)		67.6 (0.00)	C−H···O stretch
			75.7 (0.04)	C−H···O stretch
153.7 (0.04)	133.8 (0.01)	107.6 (0.03)		O−H···O stretch
153.8 (0.00)				O−H···O stretch
159.5 (0.08)	110.9 (0.05)	52.6 (0.09)	57.8 (0.11)	i.p. ring def.
		170.5 (0.12)		i.p. ring def.

[a] o.o.p. and i.p. are the abbreviations of out-of-plane and in-plane, respectively. [b] The unit of Raman activity in the parentheses is $Å^4$ amu^{-1}.

TABLE 5: Low-Frequency Raman Bands Observed in $R(\bar{\nu})$ Spectra of Gas, Liquid, and Crystalline Acetic Acid (in cm^{-1})

gas[a]	liquid	solid
106 (s)[b]	50 (s)	41 (w)
155 (w)	120 (s)	50 (s)
	170 (w)	78 (w)
		90 (w)
		124 (s)
		181 (s)

[a] Reference 39. [b] s = strong; w = weak.

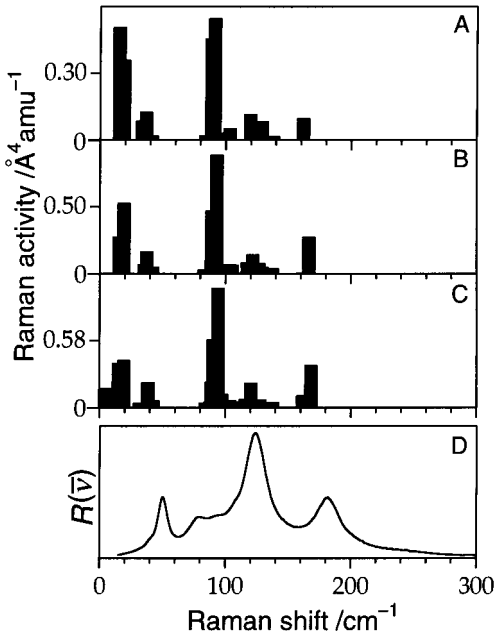

Figure 7. The $R(\bar{\nu})$ spectra in the 0−300 cm^{-1} region calculated for (A) trimer, (B) tetramer, and (C) pentamer at the HF/6-31G** level. The observed $R(\bar{\nu})$ spectrum of crystalline acetic acid at 287 K is shown in (D) for comparison.

Figure 7 shows the $R(\bar{\nu})$ spectra in the 0−300 cm^{-1} region calculated for the chain clusters at the HF/6-31G** level. The observed spectrum of the crystalline acetic acid at 287 K is also shown at the bottom. The calculated wavenumbers of the Raman active vibrations of the chain clusters in the 0−300 cm^{-1} region are collected in Table 6. Ab initio calculation provides intermolecular vibrational wavenumbers 10 ∼ 20% lower than the observed wavenumbers. All the calculated spectra in Figure 7 are decomposed into roughly four groups: strong or medium intensity bands in the 20−40 cm^{-1} region, strong bands at ≈90 cm^{-1}, weak bands in the 100−140 cm^{-1} region, and medium intensity bands at ≈165 cm^{-1}. The intensity pattern in the spectrum of the pentamer is shown to be in reasonable agreement with that in the spectrum of crystalline acetic acid, except for the positions of the weak bands calculated in the 100−140 cm^{-1} region. Although these weak bands are calculated to be higher in wavenumber than the strongest Raman active modes for the chain clusters, small bands at 78 and 90 cm^{-1} are observed on the lower wavenumber side of the strongest Raman band in the crystalline spectrum.

TABLE 6: Calculated Raman Active Low Wavenumbers (cm^{-1}) of Acetic Acid Trimer, Tetramer, and Pentamer at the HF/6-31G Level[a]**

assignment	trimer	tetramer	pentamer
out-of-plane	15.3 (0.51)[b]	15.1 (0.27)	4.3 (0.17)
	19.0 (0.36)	19.2 (0.52)	15.1 (0.39)
	36.6 (0.13)	37.4 (0.16)	19.3 (0.41)
	88.6 (0.46)	88.3 (0.10)	38.3 (0.23)
	91.0 (0.55)	89.0 (0.47)	88.9 (0.23)
		92.9 (0.88)	90.2 (0.60)
			94.3 (1.04)
in-plane	161.8 (0.10)	166.5 (0.27)	97.1 (0.12)
			161.5 (0.11)
			168.1 (0.37)
CH_3 torsion	119.6 (0.11)	121.6 (0.14)	120.5 (0.22)

[a] Vibrational modes Raman intensities of which are higher than 0.10 are shown in this table. [b] The unit of Raman activity in the parentheses is $Å^4$ amu^{-1}.

As shown in Table 6, the strong Raman bands at ≈90 cm^{-1} and the bands in the region of 20−40 cm^{-1} of the chain clusters arise from the out-of-plain rotational motions of component molecules. The bands at ≈165 cm^{-1} is attributable to the in-plain ring deformation and stretching vibrations. Although further higher wavenumber shifts are expected, these assignments can be applied to the crystalline spectrum straightforwardly. The three peaks in the crystalline spectrum at 41, 50, and 124 cm^{-1} are ascribed to the out-of-plane motions and the peak at 181 cm^{-1} is to the in-plain ring motion. The calculated bands at ≈90 and 165 cm^{-1} shift to higher wavenumbers as the aggregate size grows. Increase in the hydrogen-bonding interaction with increasing aggregation makes the force constants larger, resulting in higher wavenumber shifts. This behavior is consistent with the fact that the hydrogen-bonding energies for the chain clusters are smaller than that for the infinite chain, as suggested in *Subsection 3.A.* Stacking of the infinite two-dimensional chains along the out-of-plane axis through weak C−H···O hydrogen bonds may also cause a significant effect on the peak positions of the observed crystalline spectrum. These interactions may increase the hydrogen-bonding energy and lead to the shifts of the peak positions to higher wavenumbers.[33]

In Figure 7, the peak positions and the relative intensities in the spectra of the chain clusters show only slight changes with

increasing aggregation, except that the intensity of the strong band at ≈90 cm^{-1} relative to that of the band at ≈20 cm^{-1} apparently increases as the aggregate size grows. Although no band is seen at ≈165 cm^{-1} in the spectrum of dimer 2 (Figure 6B), the intensity pattern calculated for dimer 2, which is the dimer unit of the chain structure, is also similar to those for the other chain clusters. If a variety of sizes of the chain clusters are generated on the melting of the crystal, the weighted summation of the components therefore makes the spectrum quite broad with similar peak positions to those of the crystalline spectrum. This behavior is in agreement with the experimental observation that the melting of the crystal leads to the broadening of the $R(\bar{\nu})$ spectrum, but does not affect the peak positions so much. Depolarization ratios of the out-of plane vibrations in Table 6 are calculated to be 0.75 (depolarized) and those of the in-plane vibrations are calculated to be <0.75 (polarized). This result is consistent with the polarized Raman observation that the 50 and 124 cm^{-1} bands in the liquid are depolarized and the 181 cm^{-1} band is polarized.[20] Because the spectral features calculated for either dimer 1 or dimer 4 do not coincide with the observed spectrum, it is hard to consider that the liquid spectrum mainly arises from either of these dimer species. If dimer 1 is dominant in the liquid as in the gas phase, the bands at 106 and 155 cm^{-1} observed in the gas phase should correspond to the 120 and 170 cm^{-1} bands in the liquid, respectively (Table 5). This assumption is inconceivable because, on going from the gaseous state to the liquid state, it is unlikely that the O−H···O═C interaction of dimer 1 becomes stronger and the intermolecular vibrational bands shift to higher wavenumbers. The spectral shape for dimer 3 is not much different from those for the chain clusters, which seems to indicate that dimer 3 also contributes to the $R(\bar{\nu})$ spectrum of liquid acetic acid. The side-on dimer structures, such as dimer 3, have also been suggested as predominant species in aqueous solutions.[28−31] If liquid acetic acid consists primarily of the side-on dimer structures, the spectral shape of liquid acetic acid should be unchanged with the presence of water. However, the $R(\bar{\nu})$ spectra of acetic acid−water binary solutions cannot be reproduced by linear combinations of the pure water spectrum and the spectrum of liquid acetic acid.[21,31] Actually, the $R(\bar{\nu})$ spectrum of the acetic acid−water (1:1) mixture is well reproduced by the spectrum of dimer 3.[21,31] This result indicates that the side-on dimer structure is not dominant in the liquid state. As a consequence, comparison of the calculated and observed low frequency Raman spectra suggests that the liquid spectrum in the low wavenumber region is mainly due to the chain clusters as the fragments of the crystalline networks. The present results do not directly support the dominance of the cyclic dimers in the liquid, contrary to the previous low wavenumber studies.[18−20,22,23] Because the intensity pattern is almost unchanged with increasing temperature up to 348 K (Figure 5), a marked structural change in the liquid does not occur within the range of the temperature examined in this study.

The liquid spectrum shown in Figure 4 seems to be reproduced by taking account of the components in the crystalline spectrum plus one additional Gaussian component at 165 cm^{-1}. It is also seen that the Gaussian component at 185 cm^{-1} is much broader than the others. The observed liquid spectrum, however, cannot be reproduced properly without adding two or more such Gaussian components in the region 150−300 cm^{-1}. The broadness of the observed spectrum cannot completely exclude the contribution of other structural isomers as minor components.

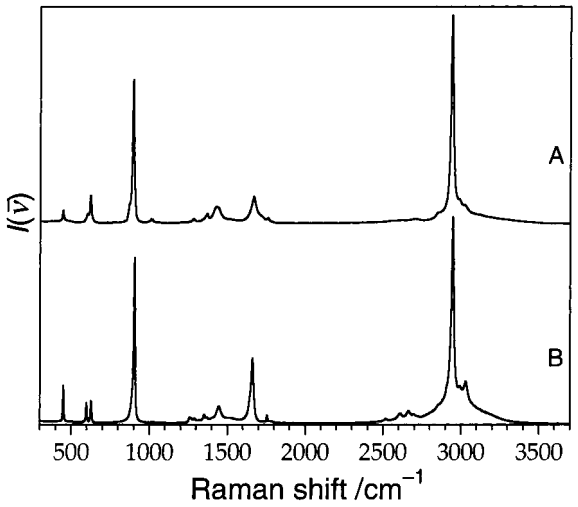

Figure 8. The $I(\bar{\nu})$ spectra of (A) liquid and (B) solid acetic acid in the 300−3700 cm^{-1} region. The intensity of each spectrum is normalized by reference to the peak intensity of the C−H stretching band at ≈2950 cm^{-1}.

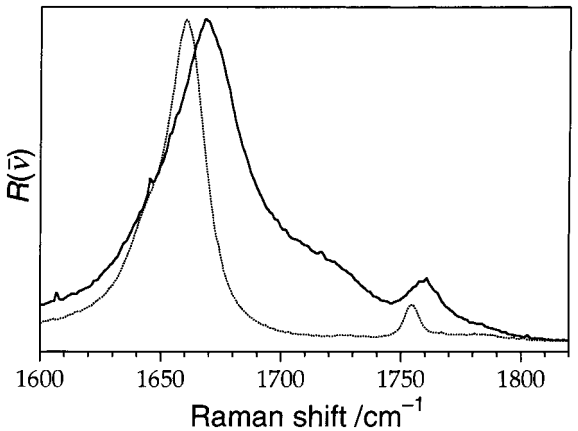

Figure 9. The $R(\bar{\nu})$ spectra of acetic acid in the C═O stretching region (1600−1840 cm^{-1}). The solid and dotted traces are recorded in the liquid and solid states, respectively. The intensity of each spectrum is normalized by reference to the peak intensity of the strong C═O stretching band at ≈1665 cm^{-1}.

3.D. Raman Spectra in Intramolecular Mode Region. Figure 8 shows the Raman spectra of crystalline and liquid acetic acid in the intramolecular vibrational region (300−3700 cm^{-1}). The features of the crystalline spectrum are similar to those of the liquid spectrum. The two prominent peaks at ≈900 and ≈2950 cm^{-1} are ascribed to the C−C and C−H stretching bands, respectively. The medium intensity band at ≈1665 cm^{-1} is safely attributable to the C═O stretching band because there is no other Raman active vibrations due to acetic acid in the 1600−1900 cm^{-1} region. Figure 9 shows the enlargement of the two spectra in the C═O stretching region. It is clearly seen that, on going from the crystalline to liquid states, the C═O band shifts slightly to a higher wavenumber (1660 cm^{-1} in the crystalline spectrum and 1666 cm^{-1} in the liquid spectrum) and becomes broadened on the higher wavenumber side exhibiting an obviously asymmetric shape. Such a high wavenumber component was found not to arise mainly from the Raman noncoincidence effect[37] from polarized Raman studies. The small band at ≈1755 cm^{-1} is seen in both the spectra.[42] Temperature dependence of the $R(\bar{\nu})$ spectra of liquid acetic acid in the C═O stretching region is shown in Figure 10. In the Raman intensity analyses at different temperatures, the best method to evaluate the relative Raman intensities is the use of

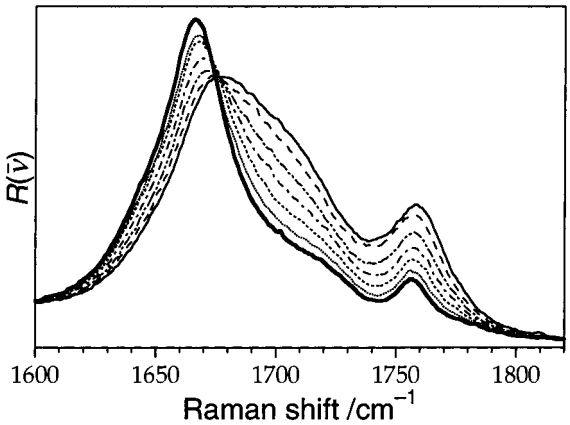

Figure 10. The $R(\bar{\nu})$ spectra of liquid acetic acid in the C═O stretching region (1600−1840 cm^{-1}) at different temperatures. The intensity of each spectrum is normalized by reference to the intensity of a band of benzene at 992 cm^{-1}. Thick-solid trace, 296 K; dotted trace, 303 K; thick-dotted trace, 313 K; dot−dashed trace, 323 K; dot-dot-dashed trace, 333 K; broken trace, 343 K; solid trace, 348 K.

TABLE 7: Calculated Wavenumbers (cm^{-1}) of C═O Stretching Modes of Acetic Acid Monomer and Cluster Species at the HF/6-31G Level[a]**

aggregate	(free) C═O str.	(H-bond) C═O str.
monomer	2038.8 (5.35)[b]	
dimer 1		1950.6 (5.60)
		1989.2 (0.00)
dimer 2	2014.4 (1.46)	1989.5 (8.29)
dimer 3	2045.2 (4.48)	2002.3 (6.13)
dimer 4		2016.4 (11.03)
		2027.5 (0.00)
trimer	2013.2 (4.45)	1956.0 (6.95)
		1997.3 (2.10)
tetramer	2011.9 (2.61)	1945.7 (9.14)
		1970.1 (0.44)
		1998.9 (5.58)
pentamer	2011.8 (3.57)	1940.9 (11.83)
		1956.5 (0.07)
		1977.5 (2.60)
		1999.6 (4.10)

[a] Wavenumbers are not multiplied by a scaling factor. [b] The unit of Raman activity in the parentheses is $Å^4$ amu^{-1}.

an internal intensity reference. By adding a small amount of benzene to liquid acetic acid (benzene mole fraction $\chi_B = 0.06$), we get a very strong Raman band of benzene at 992 cm^{-1} as an internal intensity reference in Figure 10. A small amount of benzene had no effect on the Raman spectra of liquid acetic acid in this temperature range (296−348 K). In Figure 10, the intensity of the prominent band at 1666 cm^{-1} decreases and that of the asymmetric component increases as the temperature grows. The integrated intensity of the asymmetric component becomes apparently larger than that of the prominent C═O band at 348 K. The intensity of the 1758 cm^{-1} band also becomes larger with increasing temperature. Such spectral changes with the temperatures should reflect the nature of the liquid structure of acetic acid.

Vibrational wavenumbers and Raman intensities of the C═O stretching modes calculated for the monomer and the cluster species at the HF/6-31G** level are listed in Table 7. The wavenumbers listed are not multiplied by a scale factor. Ng et al. suggested that the 1758 cm^{-1} band is due to the end C═O groups of a linear dimer and linear polymers, and the asymmetric shape around 1710 cm^{-1} in the liquid is mainly due to the monomer species.[43,44] However, the free (end) C═O groups calculated for the chain clusters have wavenumbers lower than that for the monomer. As for the chain clusters (dimer 2, trimer, tetramer, and pentamer), the calculated C═O stretching Raman active vibrations are classified into three groups: strongly hydrogen-bonded C═O groups in the 1940−1960 cm^{-1} region, weakly hydrogen-bonded C═O groups in the 1975−2000 cm^{-1}, and free C═O groups at ≈2012 cm^{-1}. These three groups show strong, strong or medium, and weak Raman intensities, respectively. This result appears to be in agreement with the liquid spectra in Figure 10; namely, the prominent band observed at 1666 cm^{-1} arises from the strongly hydrogen-bonded C═O groups of the chain clusters, and the asymmetric shape around 1710 cm^{-1} and the small band at 1758 cm^{-1} arise from the weakly hydrogen-bonded and end C═O groups of the chain clusters, respectively.

The C═O band arising from the cyclic dimer is observed at 1681.5 cm^{-1} in the gaseous state at 21 °C.[40] This result suggests that the prominent C═O band at 1666 cm^{-1} in the liquid is not due to dimer 1 because the O−H···O═C interaction is considered not to become stronger and the C═O band not to shift to a lower wavenumber on going from the gas to liquid phases. As for dimers 2, 3, and 4, the C═O modes are calculated to be 50−100 cm^{-1} higher in wavenumber than the strongest Raman active C═O mode of the pentamer. This result indicates that the strong C═O band in the liquid arises from none of these dimer species, because the prominent C═O band in the liquid spectrum is observed to be similar in peak position to that in the crystalline spectrum. If the C═O bands arising from dimers 1, 3, and 4 mainly contribute to the intensity of the asymmetric band, the structural change from the chain fragments to other cluster species should be considered in the liquid because the integrated intensity of the asymmetric band is larger than that of the prominent band at 348 K. However, as mentioned in *Subsection 3.C*, temperature dependence of the low-frequency Raman spectra suggests that the marked structural change in the liquid does not occur up to 348 K. Thus, their contributions to the asymmetric band can be thought to be small. In other words, the high-temperature components must have intermolecular configuration similar to the low-temperature one.

From the results already mentioned, we assign the strong C═O band at 1666 cm^{-1} in the liquid spectrum to the strongly hydrogen-bonded C═O groups of the chain clusters and the asymmetric shape around 1710 cm^{-1} to the weakly hydrogen-bonded C═O groups of the same cluster species. The relative intensity change in Figure 10 is therefore considered to reflect the decrease in the number of the long-chain clusters and the increase in the small-chain clusters with increasing temperature. The weak band at 1758 cm^{-1} may be attributed to the end C═O groups of the chain clusters. This band is also observed around 1758 cm^{-1} in the spectrum of acetic acid−carbon tetrachloride mixture with acetic acid mole fraction of 0.1.[46] A similar weak band has been observed in the Raman spectra of liquid acetone and acetone−carbon tetrachloride mixture and ascribed to a combination of two intramolecular modes.[45] To provide a definitive conclusion on this point, however, measurements at lower temperatures are essential.

4. Conclusions

The local structure of liquid acetic acid was studied on the basis of the temperature dependence of the Raman spectra and ab initio MO calculations on some cluster species. The melting of the crystal leads to a broadening of the low-frequency Raman spectrum, whereas it does not affect their peak positions. This constancy of the spectral positions is in accord with the similar observation in X-ray and neutron scattering measurements.

These spectral changes are well understood in the case that the liquid spectrum mainly arises from a variety of sizes of chain clusters produced on the melting of the crystal. With increasing temperature, the C═O stretching band becomes broadened toward higher wavenumbers and exhibits an asymmetric shape. The wavenumbers calculated for the C═O stretching modes suggest that the prominent C═O band is attributable to the strongly hydrogen-bonded C═O groups of the chain clusters and the asymmetric shape to the weakly hydrogen-bonded C═O groups of the same cluster species. The spectral analyses in the low wavenumber and the C═O stretching regions suggest that the chain clusters as the fragments of the crystalline networks are the predominant structures of liquid acetic acid. The spectral changes with the temperature increase do not directly support the dominance of the cyclic dimer structure in the liquid.

References and Notes

(1) Taylor, M. D. *J. Am. Chem. Soc.* **1951**, *73*, 315.
(2) Frurip, D. J.; Curtiss, L.A.; Blander, M. *J. Am. Chem. Soc.* **1980**, *102*, 2610.
(3) Karle, J.; Brockway, L. O. *J. Am. Chem. Soc.* **1944**, *66*, 574.
(4) Derissen, J. L. *J. Mol. Struct.* **1971**, *7*, 67.
(5) Almenningen, A.; Bastiansen, O.; Motzfeldt, T. *Acta Chem. Scand.* **1969**, *23*, 2848.
(6) Derissen, J. L. *J. Mol. Struct.* **1971**, *7*, 81.
(7) Jones, R. E.; Templeton, D. H. *Acta Crystallogr.* **1958**, *11*, 484.
(8) Nahringbauer, I. *Acta Chem. Scand.* **1970**, *24*, 453.
(9) Jönsson, P.-G. *Acta Crystallogr.* **1971**, *B27*, 893.
(10) Taylor, R.; Kennard, O. *J. Am. Chem. Soc.* **1982**, *104*, 5063.
(11) Desiraju, G. R. *Acc. Chem. Res.* **1991**, *24*, 290, and references therein.
(12) Holtzberg, F.; Post, B.; Fankuchen, I. *Acta Crystallogr.* **1953**, *6*, 127.
(13) Strieter, F. J.; Templeton, D. H.; Scheuerman, R. F.; Sass, R. L. *Acta Crystallogr.* **1962**, *15*, 1233.
(14) Kanters, J. A.; Kroon, J. *Acta Crystallogr.* **1972**, *B28*, 1946.
(15) Payne, R. S.; Roberts, R. J.; Rowe, R. C.; Docherty, R. *J. Comput. Chem.* **1998**, *19*, 1.
(16) Bertagnolli, H.; Hertz, H. G. *Phys. Status Solidi A* **1978**, *49*, 463.
(17) Bertagnolli, H. *Chem. Phys. Lett.* **1982**, *93*, 287.
(18) Zirnit, U. A.; Sushchinskii, M. M. *Opt. Spectrosc.* **1964**, *16*, 490.
(19) Waldstein, P.; Blatz, L. A. *J. Phys. Chem.* **1967**, *71*, 2271.
(20) Faurskov Nielsen, O.; Lund, P.-A. *J. Chem. Phys.* **1983**, *78*, 652.
(21) Kosugi, K.; Nakabayashi, T.; Nishi, N. *Chem. Phys. Lett.* **1998**, *291*, 253.
(22) Stanevich, A. E. *Opt. Spectrosc.* **1964**, *16*, 243.
(23) Jakobsen, R. J.; Mikawa, Y.; Brasch, J. W. *Spectrochim. Acta* **1967**, *23A*, 2199.
(24) Miyazawa, T.; Pitzer, K. S. *J. Am. Chem. Soc.* **1959**, *81*, 74.
(25) Kishida, S.; Nakamoto, K. *J. Chem. Phys.* **1964**, *41*, 1558.
(26) Fukushima, K.; Zwolinski, B. J. *J. Chem. Phys.* **1969**, *50*, 737.
(27) Frisch, M. J.; Trucks, G. W.; Schlegel, H. B.; Gill, P. M. W.; Johnson, B. G.; Robb, M. A.; Cheeseman, J. R.; Keith, T.; Petersson, G. A.; Montgomery, J. A.; Raghavachari, K.; Al-Laham, M. A.; Zakrzewski, V. G.; Ortiz, J. V.; Foresman, J. B.; Cioslowski, J.; Stefanov, B. B.; Nanayakkara, A.; Challacombe, M.; Peng, C. Y.; Ayala, P. Y.; Chen, W.; Wong, M. W.; Andres, J. L.; Replogle, E. S.; Gomperts, R.; Martin, R. L.; Fox, D. J.; Binkley, J. S.; Defrees, D. J.; Baker, J.; Stewart, J. J. P.; Head-Gordon, M.; Gonzalez, C.; Pople, J. A. *Gaussian 94*; Gaussian, Inc.: Pittsburgh, PA, 1995.
(28) Nash, G. R.; Monk, C. B. *J. Chem. Soc.* **1957**, 4274.
(29) Schrier, E. E.; Pottle, M.; Scheraga, H. A. *J. Am. Chem. Soc.* **1964**, *86*, 3444.
(30) Yamamoto, K.; Nishi, N. *J. Am. Chem. Soc.* **1990**, *112*, 549.
(31) Nishi, N.; Nakabayashi, T.; Kosugi, K. *J. Phys. Chem.*, to be submitted.
(32) Turi, L.; Dannenberg, J. J. *J. Phys. Chem.* **1993**, *97*, 12197.
(33) Turi, L.; Dannenberg, J. J. *J. Am. Chem. Soc.* **1994**, *116*, 8714.
(34) Faurskov Nielsen, O.; Christensen, D. H.; Have Rasmussen, O. *J. Mol. Struct.* **1991**, *242*, 273.
(35) Ishibashi, T.; Hamaguchi, H. *J. Chem. Phys.* **1997**, *106*, 11.
(36) Brooker, M. H.; Faurskov Nielsen, O.; Praestgaard, E. *J. Raman Spectrosc.* **1988**, *19*, 71.
(37) Torii, H.; Tasumi, M. *J. Phys. Chem. B* **1998**, *102*, 315.
(38) Torii, H.; Tasumi, M. *Int. J. Quantum Chem.* **1998**, *70*, 241.
(39) Egashira, K.; Nishi, N. *J. Phys. Chem. B* **1998**, *102*, 4054.
(40) Bertie, J. E.; Michaelian, K. H. *J. Chem. Phys.* **1982**, *77*, 5267.
(41) Bertie, J. E.; Eysel, H. H.; Permann, D. N. S.; Kalantar, D. H. *J. Raman Spectrosc.* **1985**, *16*, 137.
(42) The Raman measurements of an isotopic molecule ($CH_3C^{18}OOH$) confirm that all the bands observed in the 1600−1820 cm^{-1} region are due to the C═O vibrations.
(43) Ng, J. B.; Shurvell, H. F. *J. Phys. Chem.* **1987**, *91*, 496.
(44) Ng, J. B.; Petelenz, B.; Shurvell, H. F. *Can. J. Chem.* **1988**, *66*, 1912.
(45) Musso, M.; Giorgini, M. G.; Doge, G.; Asenbaum, A. *Mol. Phys.* **1997**, *92*, 97.
(46) Nakabayashi, T.; Nishi, N., unpublished results.